Medical Engineering and Physics 66 (2019) 1–11

Contents lists available at ScienceDirect

Medical Engineering and Physics

journal homepage: www.elsevier.com/locate/medengphy

Snap-valve cerebral shunt design for intracranial pressure operation and ultrasound visualization

S.C. Mitchell[a], G. Grangard[a], W. Kahouli[a], C. Dalldorf[a], A. Crain[a], E. Lee[a], A. Hamlin[a], L. Feeney[a], H. Johnstone[a], G.P. Luke[b,1], S.G. Diamond[b,2,*], D.F. Bauer[c,3,*]

[a] Dartmouth College, United States
[b] Thayer School of Engineering at Dartmouth College, United States
[c] Geisel School of Medicine at Dartmouth, Dartmouth-Hitchcock Medical Center, One Medical Center Drive, Lebanon, NH 03756, United States

ARTICLE INFO

Article history:
Received 15 July 2018
Accepted 16 December 2018

Keywords:
Cerebral shunt
Shunt valve
Hydrocephalus
Intracranial pressure (ICP)
Shunt malfunction
Ultrasound
Monitoring

ABSTRACT

Cerebral spinal fluid (CSF) shunts are the main treatment for hydrocephalus. They divert excess CSF from the ventricular system to the abdominal, pleural, or intravascular space where it is absorbed. The shunt valve regulates flow based on intracranial pressure (ICP) to maintain a physiologically stable and safe ICP. Shunt malfunction is difficult to detect, life-threatening and common. The present study demonstrates that snap-though buckling (STB) shells can be transformed into pressure-relief valves that act in the normal physiological range of ICP. Three different shell designs in this preliminary experiment were found to have opening and closing pressures that fall within the physiologically normal range of ICP of 6 to 25 cm H_2O. Furthermore, these STB shells demonstrate a valve actuation that is visible by ultrasound and have an implantable form-factor that is similar to currently available shunt valves. The unique characteristics of STB shell valves have potential clinical applications for shunt monitoring using ultrasound imaging and can be fabricated from antibiotic-impregnated materials to mitigate shunt infection. These characteristics make STB valves attractive for future use in cerebral shunt systems.

1. Introduction

Hydrocephalus is a medical condition characterized by an accumulation of cerebrospinal fluid (CSF) in the brain. This accumulation is due to obstruction of the circulation of CSF or an imbalance in either production or absorption of CSF. Hydrocephalus may be caused by congenital brain defects, tumors, infection, or intraventricular hemorrhage [1]. Accumulation of CSF eventually leads to a life-threatening increase in intracranial pressure (ICP) above the normal physiologic range of 6–25 cm H_2O [2,3].

The current mainstay of treatment for hydrocephalus is a surgically implanted CSF shunt [4,5]. A CSF shunt consists of a proximal silastic catheter placed into the ventricular system, a valve that regulates the flow of CSF through the shunt based on ICP, an optional anti-siphon device that prevents siphoning of CSF when a patient is upright, and a distal catheter placed into a body cavity that can easily absorb the diverted CSF [6]. The most common terminus for the distal catheter is the peritoneal cavity, however shunts have been placed into the pleural cavity, venous system (typically internal jugular vein or common facial vein) [7], and even gallbladder [8] or urinary bladder [9]. Shunt valves are typically designed to continuously divert CSF as needed to maintain the ICP in a normal physiological range of 6–25 cm H_2O [2,3]. In the United States, hydrocephalus is the most common pathology surgically treated by pediatric neurosurgeons. Hydrocephalus accounts for 0.6% of all pediatric hospital admissions, and 3.1% of all pediatric hospital costs ($1.4–2.0 billion) [10].

Shunt systems fail at the alarming rate of 40% in the first year [11] and about 4.5% per year thereafter [12], with a failure rate as high as 81% after 12 years [13]. Shunt malfunction mechanisms include infection (11–23%) [5,14,15], over drainage (3.5%) [11], obstruction by intraventricular debris, ingrowth of microglia, astrocytes or choroid plexus (56.1%) [16], tubing disconnection or fracture (13.6%) [13]. Approximately 73% of shunt malfunctions effect the flow of CSF through the shunt via obstruction or over drainage [13,17], resulting in symptoms of either increased or decreased ICP, respectively.

It is difficult to diagnose shunt malfunctions early because symptoms vary in onset and acuity. Symptoms often develop over hours to days, with some patients rapidly developing severe

* Corresponding authors.
E-mail address: David.F.Bauer@hitchcock.org (D.F. Bauer).
[1] https://engineering.dartmouth.edu/people/faculty/geoffrey-luke.
[2] https://engineering.dartmouth.edu/people/faculty/solomon-diamond.
[3] https://geiselmed.dartmouth.edu/faculty/facultydb/view.php/?uid=6012.

https://doi.org/10.1016/j.medengphy.2018.12.024
1350-4533/

symptoms and some patients maintaining mild symptoms for longer periods of time. Symptoms of decreased ICP due to over drainage include neck pain or stiffness, nausea, and vomiting [18,19]. Elevated ICP due to shunt obstruction in an infant, initially causes a rapidly enlarging skull and head circumference because the skull bones are not yet fused, rather are connected by fibrous sutures that allow for the rapid brain growth in early childhood [20]. For older children and adults whose skulls bones have fused, however, symptoms of shunt obstruction and elevated ICP begin with subjective symptoms such as headache, nausea, abdominal pain and lethargy, irritability [21], and progress to more objective symptoms such as vertigo, emesis [22], somnolence [23], seizures, vision loss [24], bradycardia, loss of consciousness, and death [25–27] if left untreated. Early symptoms can be mild and can overlap with other diagnoses such as migraine, stress or tension headache, infection such as influenza or gastroenteritis, or other etiology that has headache and nausea as part of its symptomatology making early diagnosis of shunt failure difficult.

Children under three years of age and children with developmental delay are more likely to suffer morbidity and mortality from undiagnosed elevated intracranial pressure. This is thought to be due to the inability of these populations to effectively communicate the early subjective symptoms of elevated ICP prior to the development of more serious objective signs and symptoms [10]. Objective symptoms associated with shunt malfunction include bulging fontanel, fluid collection along the shunt, abnormal shunt pump test, and accelerated head circumference growth [28].

The standard clinical paradigm for identifying shunt malfunction requires onset of worrisome symptoms before patients seek medical attention [29]. Intrinsic methods for continuous monitoring of shunt systems are currently unavailable. Medical providers attempt to diagnose shunt malfunction through clinical assessment, physical examination, imaging studies and invasive procedures [30]. Comparative imaging studies may be used to asses for ventricular enlargement including ultrasound via the anterior fontanel in infants, or computed tomography (CT) and magnetic resonance imaging (MRI) in children and adults [6]. However, in as many as 36% of cases there is no consistent ventricular dilation during episodes of shunt malfunction making imaging an unreliable predictor of shunt malfunction [31]. Radiographs can evaluate the course of the shunt system for fracture or disconnection that can cause obstruction [6,26]. Invasive diagnostic procedures include shunt reservoir tap to evaluate for function or infection, ICP monitoring with implantation of a fiberoptic strain gauge, or a nuclear medicine “shunt-o-gram” to evaluate for flow through the shunt [32]. Shunt malfunction is often not recognized early because of the poor sensitivity and specificity, and poor positive and negative predictive value of these tests.

Many factors combine to make assessment of CSF shunts very challenging. An early warning system that could reliably identify lack of flow through a shunt system and then notify a physician or caregiver would be a major advance in safety for the treatment of hydrocephalus.

This work evaluates the feasibility of a snap-valve that could be used to directly assess and detect the presence of flow through a CSF shunt. Such a device could significantly lessen uncertainty surrounding shunt malfunction, decrease the danger of delayed medical attention, reduce medical costs associated with shunt diagnostic procedures, and shift the shunt diagnostic paradigm towards preventative care. Furthermore, a valve manufactured from antibiotic-impregnated materials could reduce rates of infections that cause many shunt malfunctions, further decreasing perioperative complications. This novel mechanism may eventually permit definitive detection of shunt blockage prior to the onset of symptoms.

2. Background

2.1. STB shell technology

Pressure-loaded elastic spherical shells exhibit interesting mechanical properties. They have static stability, but when there is a pressure difference across the shells, they can become unstable and buckle into an inverted geometric conformation. This phenomenon is called snap-through buckling (STB). When the pressure difference is reduced, the shells rebound into their original conformation. The theoretical pressure difference at which STB occurs for a symmetrical shell is described by

$$\Delta p = 2E\frac{h^2}{R^2}\sqrt{3\left(1-\upsilon^2\right)}, \tag{1}$$

where Δp denotes the STB pressure difference across a thin spherical shell, E is the Young's modulus, h is the thickness of the shell, R is the radius of the shell and υ is the Poisson's ratio. The boundary conditions are with no initial vertical displacement and the base of the structure clamped to a wall [33].

2.2. Current medical application of STB technology

Although STB devices are not currently used in cerebral shunts, these devices are used in other medical implants. For example, the ventricular assist device (VAD) produced by INCOR, Inc. (Berlin, Germany) relies on a pneumatically actuated free-floating shell to transfer the pneumatic pressure to the blood. The shell constitutes an interface between the blood and the pneumatic chambers. This internal shell has a deformation mechanism that is repeated every time the ventricular assist device pulsates. An average heart beats about 115,200 times per day, and this polyurethane VAD has proved to be durable and reliable for this medical application [34] suggesting that STB shells have reliability over a large number of cycles and for use in biomedical applications. The key challenge in adapting STB devices to the cerebral shunt application is to achieve valve characteristics and ensure operation at physiological ICP pressures.

2.3. STB valve for hydrocephalic shunting

The proposed device for application in cerebral shunts is a STB shell that acts as a relief valve placed in series with the flow of CSF. The STB (valve opening) and rebound (valve closure) events of the shell can be designed to occur at thresholds below 25 cm H_2O and above 6 cm H_2O respectively. At normal ICP, the shell is in the relaxed or closed state. As CSF accumulates in the cranium, the ICP increases according to the rules of cerebral compliance applying mounting pressure on the convex surface of the shell (Fig. 1A). Finally, the ICP reaches a critical threshold, resulting in a STB event that opens the shell (Fig. 1B). The opening in the shell drains fluid from the ventricle to the distal end of the catheter, decreasing ICP until the shell rebounds to its original closed position when ICP is at the rebound pressure (Fig. 1C). Thus, the shell acts as a valve by opening a hole in the shell at a distinct pressure and closing the hole at the rebound pressure. Dynamic permeability is the term used to describe the ability for the shell to block flow (impermeable) in one conformation and to allow flow (permeable) in its inverted conformation.

A small form-factor shell and housing is imperative for incorporation into an implantable device due to space constraints. Two concepts for *in vivo* valve housings are depicted in Fig. 2. Future shell designs will likely be housed in an injection-molded component.

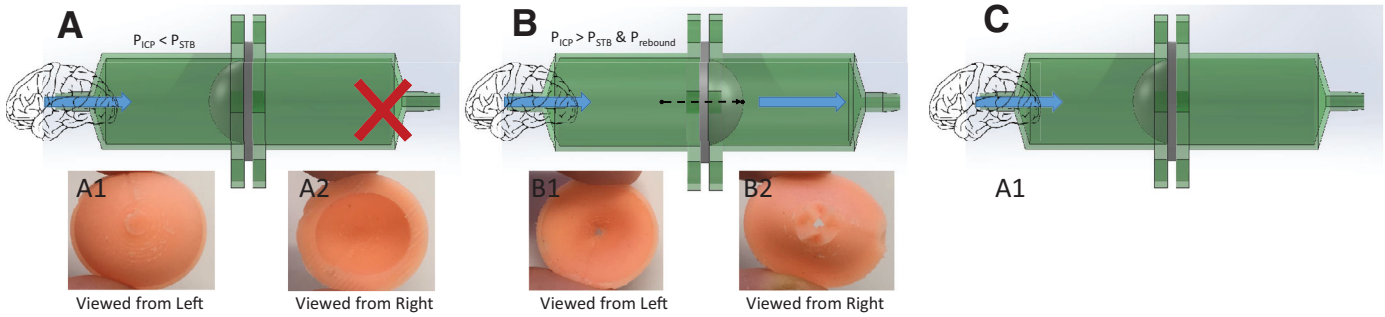

Fig. 1. Schematic and prototype demonstration of the concept of dynamic permeability for a STB valve using the four spoke method. Solid arrows indicate direction of CSF pressure and flow from the brain to the abdomen. (A) Pressure to the left is below the STB event pressure making the shell impermeable. Impermeable shell state as viewed from the left (A1) and from the right (A2). (B) Pressure is above the STB pressure causing the shell to change its conformation. Permeability is exhibited with inlet on the left and outlet on the right in B1 and B2, respectively. (C) The dashed arrow indicates the rebound phase of the cycle, and may cause backflow or pressure in the catheter system (see discussion Section 5.5).

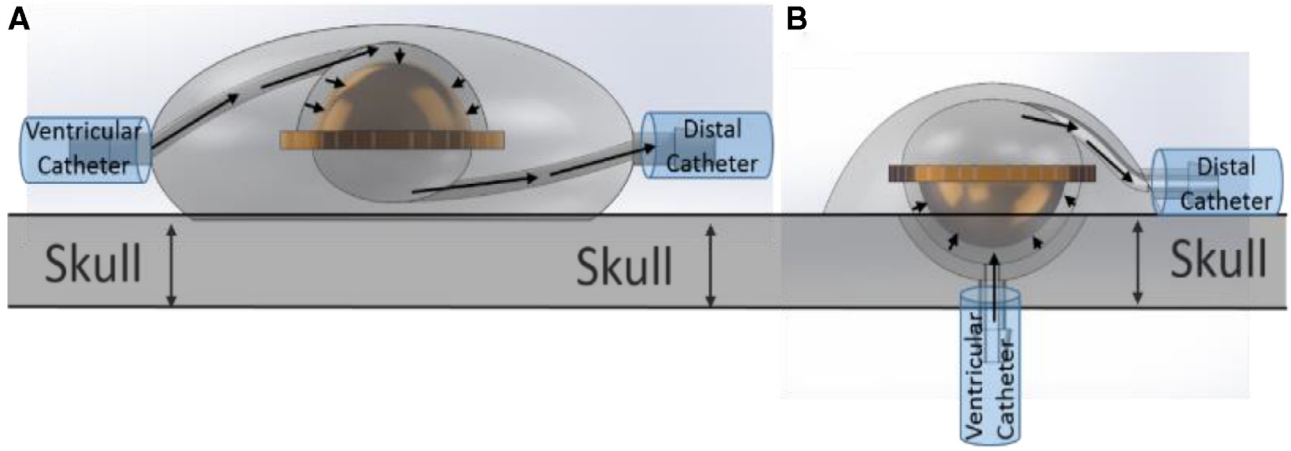

Fig. 2. Two concepts for *in vivo* valve housings. Long arrows indicate the direction of flow, short arrows indicate the pressure applied to the surface of the shell in the closed position. (A) Concept 1: the entire housing is located above the skull; (B) Concept 2: The housing is designed to decrease the profile above the skull by occupying a portion of the bur hole.

3. Methods

3.1. Shell design, fabrication and permeability

Several shell parameters were tested to determine the effects of design parameters on the behavior of the valve, and to allow for future optimization of shells that have small form-factor designs while achieving the opening and closing pressure requirements for cerebral shunts. Parameters included shell thickness, radius, and material hardness. Shell dimensions are defined in a cross section of a generic shell (Fig. 3).

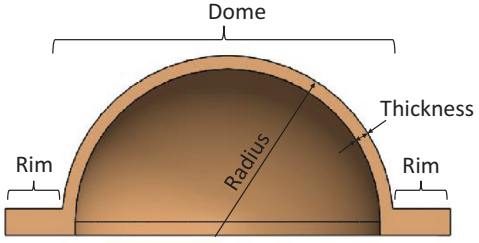

Fig. 3. Shells consist of a rim and a dome. Rim dimensions were constant with length × height of 4 mm × 2 mm. Dome dimensions varied by radius and thickness for different experiments. The depicted shell has a radius of 10 mm and thickness of 1 mm for visual reference.

Shells consist of two parts: a rim for securing the shell in position, and a dome which is the active portion of the shell exposed to the testing pressure and environment. All shells had consistent rim dimensions of 4 mm × 2 mm. All shells had hemispheric domes. Dome dimensions were varied and include three different shell dome thicknesses: 0.5 mm, 0.75 mm, 1 mm, and three shell dome diameters 50 mm, 75 mm, 100 mm. All shells were fabricated from one of the SMOOTH-ON (Smooth-On Inc., Macungie, PA) Platinum Cure [35] silicone series, selected for the Shore Harnesses properties (Table 1).

3.2. Shell fabrication

All molds were designed using SOLIDWORKS (Dassault Systemes, Inc.,Vélizy-Villacoublay, France) software. Shells were fabricated using 3D printed molds acquired from ProtoLabs (Maple Plain, Minnesota) WaterShed XC 11,122 High-Resolution Stereolithography built in 0.002 in layers. SMOOTH-ON silicone was mixed and then poured and pressed by hand into the mold. After fabrication, quality control excluded shells which contained bubbles, or were asymmetric to the touch or by sight.

3.3. Opening/closing pressure recording

STB event pressures were evaluated by securing the shell into a testing apparatus then applying water pressure to the convex face of the relaxed shell using a column of water (COW) over the range of STB and rebound event pressures for each shell following

Table 1
A summary of the materials used to fabricate the shells. Hardness varied from 00–30 to Shore 45A. All were platinum cure silicon materials selected only for their material hardness properties.

Shore Hardness	00–30	18A	25A	30A	40A
SMOOTH-ON Product Series	ECOFLEX®	SORTA-Clear®	Rebound 25™	Mold Star®	Rebound 40d™

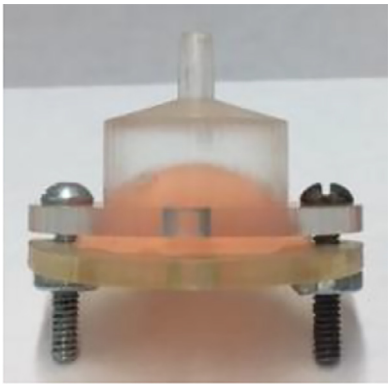

Fig. 4. An example of a shell loaded into the testing apparatus. The shell rim is clamped in place preventing leaks from the side of the apparatus and securing the shell in place.

the outlined technique below. The testing apparatus consisted of a small fluid filled chamber, on the convex side of the shell. The shells were secured by clamping the rim of the shell between the chamber and a clamping disc of the testing apparatus with nuts and bolts which were tightened by hand to ensure a watertight seal (Fig. 4). The concave side of the shell was exposed to room air. The COW was sourced by a beaker of water, which was elevated or lowered at an approximate rate of 2–5 cm/s. The COW pressure was transferred through a 3 mm inner diameter flexible IV tubing to the testing apparatus to the face of the shell. To simulate increasing ICP, the beaker was steadily raised to increase the COW pressure. When the shell underwent a deformation and began to drain water through the outlet of the test apparatus, the height of the COW was recorded to +/- 0.5 cm H_2O accuracy from the rim of the shell as the "STB pressure". To simulate the relative decrease in ICP with the drainage of CSF, once the shell opened, the beaker was lowered until the shell rebounded to the closed position and no fluid flowed and was recorded as the "rebound pressure".

3.4. Dynamic permeability attempts

The elastic shell domes were inflicted with a variety of intentional defects penetrating the entire thickness of the dome in attempts to achieve dynamically permeable behavior using the STB phenomenon. Defects were inflicted after shell fabrication by hand using an X-Acto knife.

3.5. Shell defects, thickness, radius and hardness effects on STB and rebound event pressures

Miniaturized STB shells were tested for STB and rebound pressures at physiologically normal ICP to assess the practicality of using them in a shunting application. All shell valves were inflicted with four orthogonal spokes of 1.1 mm length in a "+" shaped defect at the apex of each shell, converting the shell to a shell valve. Spokes were made with a custom-made die cutter for precision and reproducibility. Spoke length was 1.1 mm originating from the apex of the dome.

3.5.1. Defects

One Rebound 25A and one Sorta-Clear 18A shells, each with dome thickness of 1 mm and radius of 10 mm, were tested for their STB and rebound pressures before and after being inflicted with a slit defect. Each shell was placed in the testing apparatus, tested for one STB and rebound event pressure, then removed from the testing apparatus 10 separate times to account for error in the clamping procedure. The mean of the 10 STB and closing pressure recordings for each shell before and after defect, respectively, were then compared using unpaired, two-tailed *t*-tests assuming unequal variance.

3.5.2. Thickness testing

Three groups of three shells each were made with each shell thicknesses, 0.5, 0.75, and 1 mm were tested keeping material (Rebound 40), and diameter (10 mm) constant. Five STB and rebound event pressures were recorded for each of the three shells in each group. The STB and rebound data were lumped for each group respectively, and one-way ANOVA performed. The means for each group were then compared with a best fit line.

3.5.3. Radius testing

Three groups of two shells each were made with different radii, 5 mm, 7.5 mm, and 10 mm, keeping material (Ecoflex 00–30) and thickness (1 mm) constant. Five STB and rebound event pressures were recorded for both shells in each group. The STB and rebound data were lumped as 10 data points respectively for each group, and one-way ANOVA performed. The means for each group were then compared with a best fit line.

3.5.4. Hardness testing

Shore Hardness is commonly used to characterize the material properties of elastomers and is related to the modulus of elasticity [36,37]. Three groups of three shells each were made with different Shore Hardness values of 18A, 30A, and 40A, keeping radius (100 mm) and thickness (1 mm) constant. The mean STB and rebound pressures were recorded for each trial and the standard deviation was calculated from the cumulative 15 STB events of each group of shells. The means for each group were then compared with a best fit line.

3.6. Flow rates

Flow rate of water though the "+" shaped 1.1 mm spoke defects was tested using a Rebound 25A 0.5 mm thick and 10 mm radius dome. Pressure was applied such that STB event occurred and the valve opened, and pressure was then adjusted to the recording pressure. Eight data points were collected over a range from 5.5 to 110 cm H_2O. Flow rate was determined by weighing the mass of water that flowed through the valve opening in one minute.

3.7. Cycle reliability testing

To function as a shunt valve with a practical lifecycle, a STB shell must withstand a high number of STB and rebound events without significant changes to its event pressures. STB events of one Rebound 25, 0.75 mm thickness shell were tested for consistency at room temperature in 3 g/l saline for over 42,000 cycles

using a Standard Infuse/Withdraw Pump 11 Elite Programmable Syringe Pump (Harvard Apparatus Inc., Holliston, MA) programmed to oscillate 3 mL of fluid at a rate of 1 mL/s. The cycling was paused and STB and closing pressures were evaluated at approximately 2000 cycle intervals using the method described above. The number of STB cycles was recorded using an optical interruption sensing prototype and verified by the onboard pump cycle display.

3.8. Ultrasound monitoring

Monitoring of the shell valve with ultrasound was performed with a Vantage 256 (Verasonics, Inc., Kirkland, WA) system with the GE L3-12-D Linear Array transducer at a frequency of 6.25 MHz. The test apparatus was placed in a water phantom and the shell (Rebound 25, thickness 1 mm, radius 10 mm, four radial spokes of 1.1 mm length) was observed directly from the convex side of the relaxed shell, such that the STB event would occur towards the transducer.

4. Results

4.1. Dynamic permeability

Dynamic permeability resulting in a clear path of flow was demonstrated in $n \geq 2$ nonlinear, spoke-like slit defects that intersected at or near the apex of the shell. Spokes intersecting at the apex exhibited a larger opening. Single slit defects did permit flow upon STB, but did not provide a clear path to flow in the permeable state resulting in a very significant reduction of the rebound pressure, which is not desirable for shunting applications. A summary of defects is shown in Fig. 5.

4.2. Shell defects, thickness, radius and hardness effects on STB and rebound event pressures

4.2.1. Defect testing

The Rebound 25A shell prototype before spoke defects had an STB pressure of 114 ± 5.5 cm H_2O and rebound pressure of 30.4 ± 2.0 cm H_2O (average of 10 trials). After introducing a spoke defect, the STB pressure was statistically unchanged at 115.1 ± 7.5 cm H_2O ($t(16) = -0.36$, $p = 0.73$, $N = 20$, unpaired, two-sample, two-tailed, unequal variance t-test), and the rebound pressure on the same Rebound 25A shell decreased to 27.8 ± 3.0 cm H_2O ($t(15) = 2.27$, $p = 0.04$, $N = 20$).

Likewise, the Sorta-Clear 18A shell prototype without spoke defects had and STB pressure of 41 ± 4.4 cm H_2O and a rebound pressure of 14 ± 1.3 cm H_2O (average of 10 trials). After addition of spoke defects, the STB pressure was statistically unchanged at 42 ± 3.0 cm H_2O ($t(16) = -0.41$, $p = 0.69$, $N = 20$) and the rebound pressure statistically decreased to 10 ± 2.0 cm H_2O after addition of spoke defects ($t(16) = 5.85$, $p < 0.01$, $N = 20$) using an unpaired two-tailed t-test assuming unequal variance.

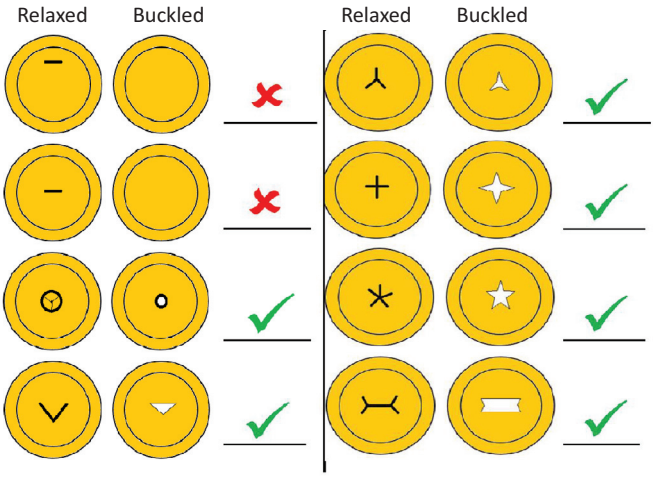

Fig. 5. Depictions of attempts to achieve dynamic permeability. Penetrating defects are depicted as bold black lines. The relaxed state of the shell and the ensuing deficit appearance when the shell is in the buckled conformation is depicted with white depicting a clear path for fluid flow. If the defect resulted in dynamic permeability, it is marked with a "√", if not, the configuration received a "✗". Intersecting spokes connecting at least two nonlinear points at or near the apex resulted in dynamic permeability.

Table 2
Mean STB ± standard error of the mean and rebound pressures ± standard error of the mean for shells of differing only by thickness.

Thickness (mm)	Mean STB Pressure ± SE (cm H_2O)	Mean Rebound Pressure ± SE (cm H_2O)
1.0	190 ± 2.4	62 ± 0.4
0.75	105 ± 2.4	31 ± 0.4
0.5	39 ± 2.5	15 ± 1.2

Table 3
Mean STB ± standard error of the mean and rebound pressures ± standard error of the mean for shells of differing only by radius. Shells composed of 7.5 and 10 mm radii, exhibit STB and rebound event pressures that lie within the physiologically normal range for ICP.

Radius (mm)	Mean STB Pressure ± SE (cm H_2O)	Mean Rebound Pressure± SE (cm H_2O)
5	36 ± 2.2	23 ± 1.6
7.5	23 ± 1.3	10 ± 0.7
10	15 ± 0.2	7 ± 0.1

4.2.2. Thickness testing

One-way ANOVA indicated that the means for the three groups of shells of 1.0, 0.75, 0.5 mm thickness for each shell type were not the same for STB pressure ($p < 0.01$) or for rebound pressures ($p < 0.01$). Average values of STB and rebound events appear to correlate with the square of the shell thickness ($R^2 = 0.99$ and 0.99, respectively) as predicted by Eq. (1) (Table 2) (Fig. 6).

4.2.3. Radius testing

One-way ANOVA indicated that the means for the three groups of shells of 10, 7.5, and 5 mm radius were not the same for STB pressure ($p < 0.01$) or for rebound pressures ($p < 0.01$). Average STB and rebound event pressures for each shell type appear to follow a linear trend ($R^2 = 0.98$ and $R^2 = 0.99$, respectively) with the inverse square of the radius of the shell as predicted by Eq. (1) (Table 3) (Fig. 7).

4.2.4. Hardness testing

One-way ANOVA indicated that the means for the four groups of shells of various Shore hardness were not the same for STB pressure ($p < 0.01$) or for rebound pressures ($p < 0.01$). Average STB and rebound for each shell type were found to correlate ($R^2 = 0.98$ and 0.99) (Fig. 8) in direct proportionality with the Shore hardness of the shell (Table 4).

4.3. Flow rate

Flow rate though the open valve was recorded and appeared to be linearly proportional to the COW pressure (Fig. 9). It was noted that the two lowest pressure data points demonstrated a possible deviation from the linear trend present in the higher-pressure flow readings. This may suggest that at pressures just before a rebound event the shell begins to flex back towards a more neutral position

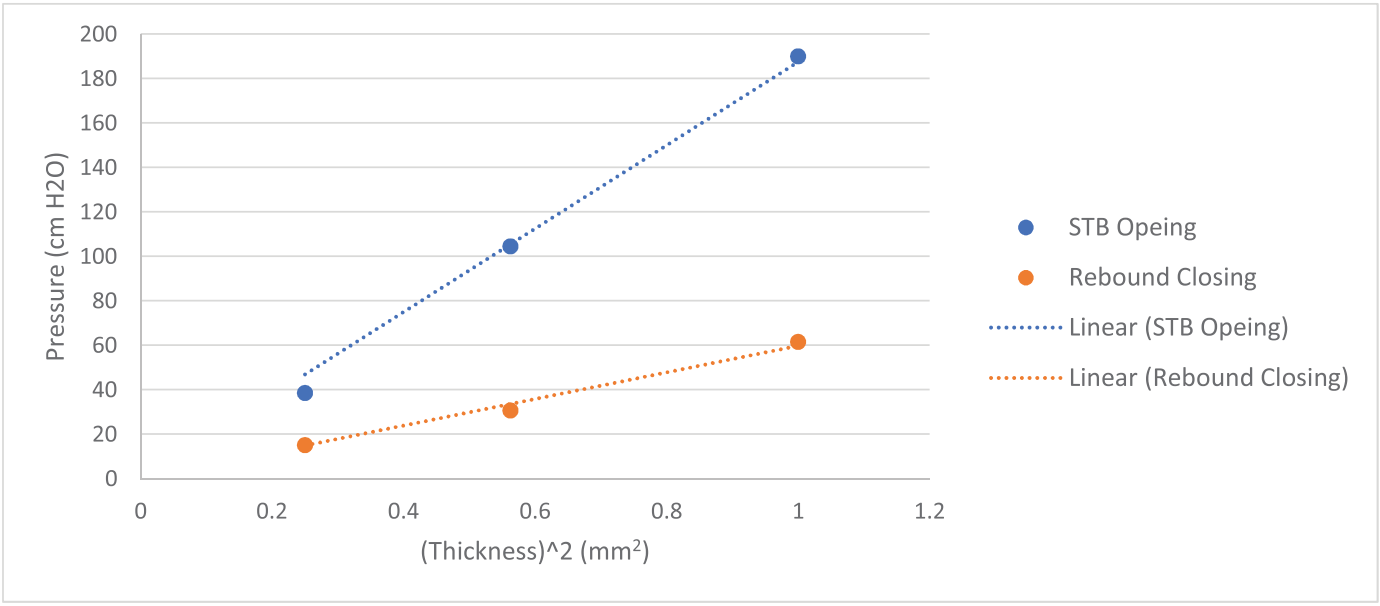

Fig. 6. Effect of dome thickness on the STB and rebound pressures of the shells fit with a linear regression (R^2 = 0.99 and 0.99, respectively).

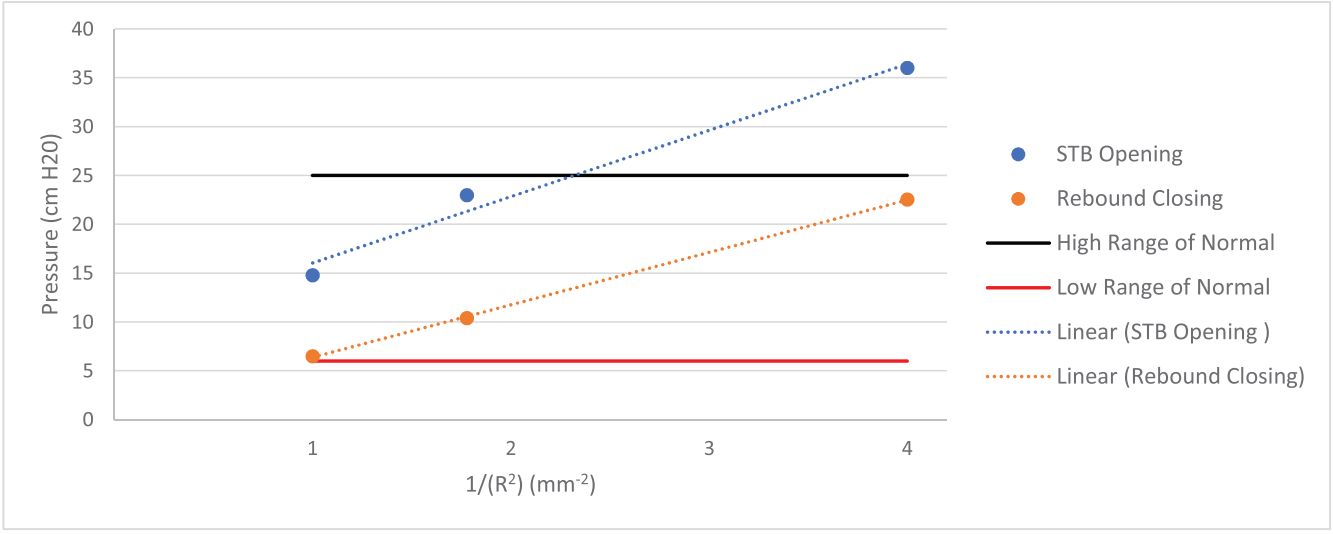

Fig. 7. Effect of dome radius on STB and rebound pressures fit with linear regressions (R^2 = 0.98 and 0.99, respectively). Horizontal lines indicate the high (solid black) and low (solid red) values of normal ICP. (For interpretation of the references to color in this figure legend, the reader is referred to the web version of this article.)

Table 4
Mean STB ± standard error of the mean and rebound pressures ± standard error of the mean for shells of differing only by hardness.

Harness	Mean STB Pressure ± SE (cm H_2O)	Mean Rebound Pressure ± SE (cm H_2O)
Shore 18A	25 ± 1.1	15 ± 0.6
Shore 25A	94 ± 1.4	33 ± 1.6
Shore 30A	113 ± 0.9	38 ± 1.6
Shore 40A	186 ± 2.3	62 ± 0.4

thus effectively decreasing the size of the opening and reducing flow rate. More data and quantitative visual inspection of the valve opening would need to be performed to validate this theory.

4.4. Cycle reliability testing

Cycles: The average across 42,000 STB and rebound pressures were 92.9 and 33.8 cm H_2O respectively with standard deviations of 0.4 and 0.5 cm H_2O respectively. First and last cycles had the same recorded STB and rebound event pressures figure (Fig. 10).

4.5. Ultrasound monitoring

The two distinct states, relaxed and deformed, of the shell were distinguishable from one another using ultrasound imaging (Fig. 11).

5. Discussion

To have potential for cerebral shunting, STB shells must convert effectively to valves, serve in the physiologic pressure range of 6–25 cm H_2O, have a small form-factor for implantation similar to currently available products, and operate reliably over many cycles. This study demonstrates that these requirements can be achieved using STB shells.

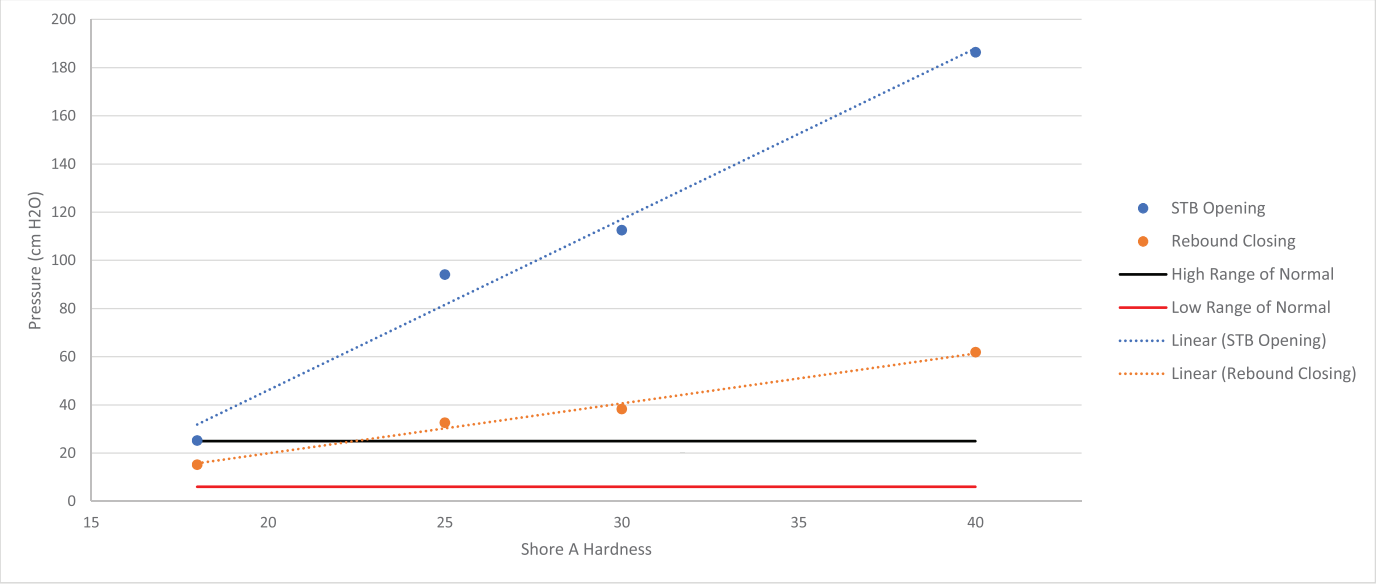

Fig. 8. Effect of shell material hardness on STB and rebound pressures fit with linear regressions (R^2 = 0.98 and 0.99, respectively). Horizontal lines indicate the high (black) and low (red) range of normal ICP. (For interpretation of the references to color in this figure legend, the reader is referred to the web version of this article.)

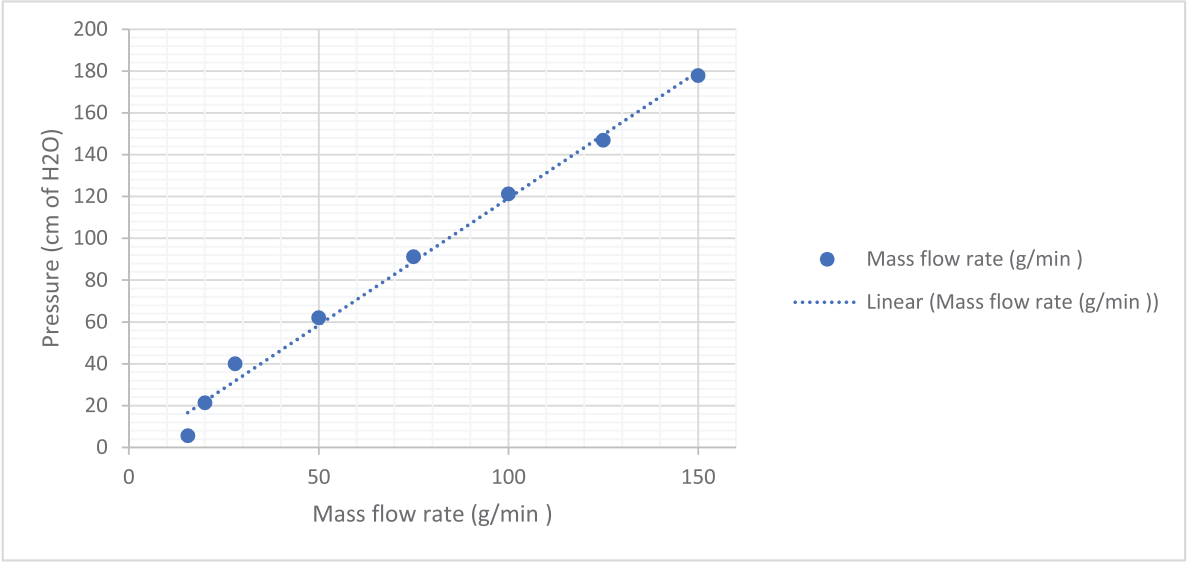

Fig. 9. Mass flow rate through an open Rebound 25A 0.5 mm thick and 10 mm radius dome at different pressures demonstrated a linear relationship (R^2 = 0.99).

5.1. Dynamic permeability

Shell do not demonstrate statistically significant differences in STB pressures after inflicting spoke defects (Rebound 25: $t(18) = -0.36$, $p = 0.73$; Sorta Clear 18A: $t(18) = -0.41$, $p = 0.69$), however, the rebound pressures for both shells do demonstrate statistically significant lower STB pressures after inflicting spoke defects (Rebound 25: $t(18) = 2.28$, $p = 0.04$; Sorta-Clear 18A: $t(18) = 5.58$, $p < 0.01$). This makes sense because in the closed configuration, under compressive loading the shell stress is transmissible across the defect to the adjacent portion of the shell through contact, however in the open configuration, part of the tensile energy stored in the material at the apex is lost at the opening. This may explain the resulting loss of a portion of the spring like properties of the elastic at the opening that typically supply rebound force. This is important for understanding how the shells behave and has implications for quality control of closing pressures as well. Shells must be tested and verified for STB and rebound pressures after the slit defect has been imposed for accurate and reliable measurements.

5.2. Shell parameters

Shell parameter testing results for thickness, radius and material hardness in shells with slit defects demonstrate trends that verify the relationships of proportionality for STB found in previous theoretical work without slit defects: most notably that the STB event pressure is directly proportional to the hardness of the shell material, the square of the thickness of the dome and inversely proportional with the square of the radius of the shell

$$P_{STB} \propto E\frac{h^2}{R^2} \quad . \tag{2}$$

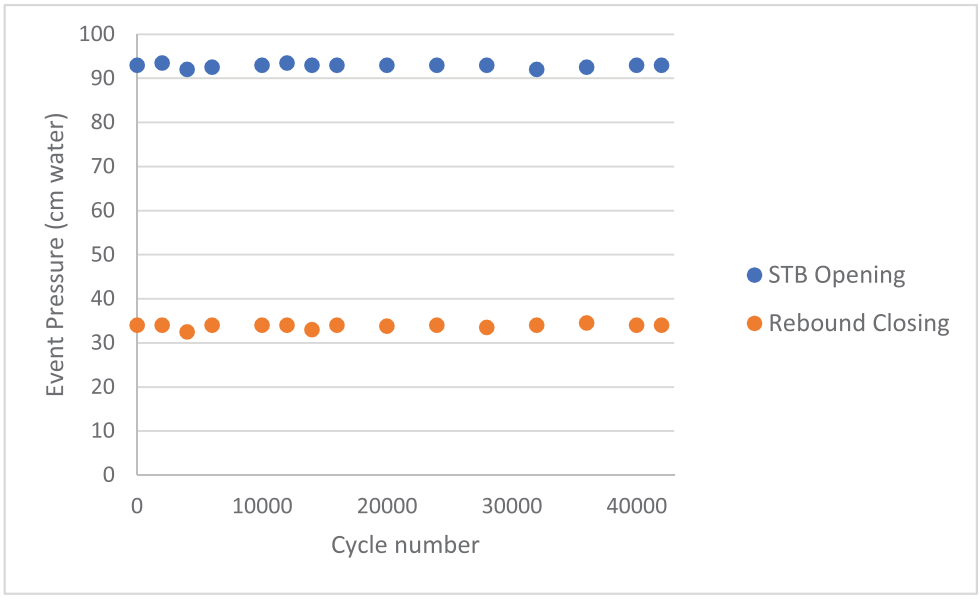

Fig. 10. STB and rebound event pressures over 42,000 cycles showing stable event pressures.

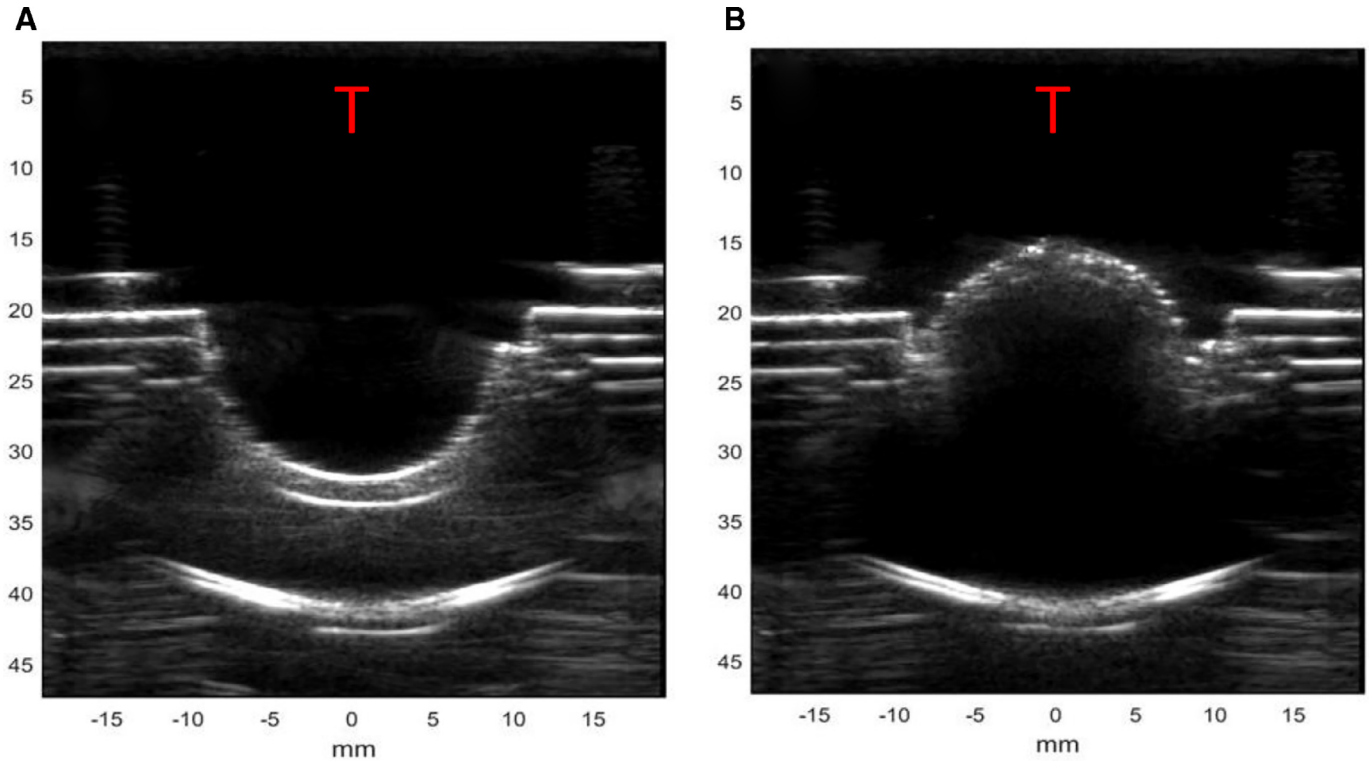

Fig. 11. Ultrasound imaging of the valve with transducer marked with "T" in: (A) closed shell state after rebound event and before STB event, and (B) open shell state after STB event are clearly differentiated using ultrasound visualization. Although not well visualized, the shell defect becomes noticeable as an interruption of the smooth surface in the open shell state at the apex of the inverted shell.

Interestingly, our results also showed similar relationships for rebound pressures

$$P_{rebound} \propto E\frac{h^2}{R^2}. \quad (3)$$

Understanding and verifying the parameters effecting STB and rebound events pressure has already allowed production of shells that open and closes in the physiological range of ICP (6–25 cm H_2O). Shell parameters of 00–30 material, 1 mm thickness and either 7.5 mm and 10 mm radius had average STB pressures of 23.0 ± 1.3, and 10.4 ± 0.7 cm H_2O and closing pressures of 14.8 ± 0.2, and 6.5 ± 0.1 cm H_2O respectively. Additionally, shells made from Shore 18A hardness with a radius of 10 mm and thickness or 1 mm had STB pressures of 25 ± 1.1 and rebound of 15 ± 0.6 cm H_2O. These results prove that many different options for shell parameters that can be used to achieve the pressure requirements and that these parameters do not lie at extreme limits of material or manufacturing capabilities. In the future, shells of even smaller radius can be designed to fulfill the CSF pressure requirements while also maintaining an even smaller form factor than

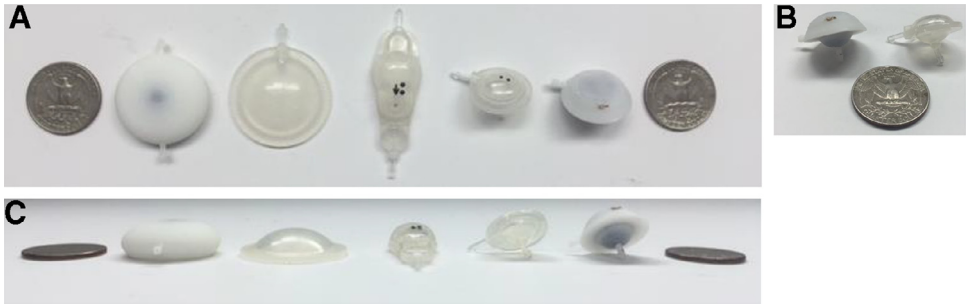

Fig. 12. Images depicting potential implantable housing of the 5 mm radius STB valve. (A,B) Different views of concepts and state-of-the-art valves. Order left to right: quarter, 3D mockup of Concept 1 (presented in Fig. 2), Integra NeuroCare (Plainsboro, NJ) Ommaya CSF reservoir, Medtronic (Minneapolis, MN) Strata valve, Integra (Plainsboro, NJ) Pudenz Flushing valve, 3D Mockup of Concept 2 (presented in Fig. 2). (C) Direct Comparison of Concept 2 (presented in Fig. 2) vs. Integra (Plainsboro, NJ) Pudenz Flushing valve with a quarter for reference.

Table 5
The range of possibilities for volume of CSF drainage per day approximate the number of cycles that the valve would experience per unit time. Valves were tested for reliability over a number of cycles that approximate between 197 *in vivo* days to 143 *in vivo* years depending on the rate of drainage of the individual.

Patient CSF drainage characteristics	Total drain/day (ml)	Openings/day	Time open/day (min)	*In vivo* time to 42,000 cycles
Low volume	2.4	0.8	0.2	143 years
Avg. volume	194.4	64.8	15	1.8 years
High volume	638.4	212.8	49	197 days

current shells by further reducing the hardness and thickness of the shells. For example, shells designed with a radius of 5 mm can be incorporated into valve casings that have similar form factor to currently used valves, and it is possible for even smaller shells to be made (Fig. 12).

5.3. Flow rate and reliability testing

ICP is related to the intracranial volume by the Monro–Kellie doctrine [38]. As the volume of material in the skull increases, the ICP rises. The specific drainage volume from shunts varies depending on the patient from a minimum of about 2.4 ml to a maximum of 736 ml per day, with the average patient draining 194 mL per day [39]. This equates to flow rates of 0.0017 to 0.4417 ml/min. Accurate flow detection at this rate is extremely difficult. Data from infusion studies conducted by Kasprowicz et al. suggest that, on the order of 3 mL increase or decrease in CSF volume corresponds to a change in ICP from 10 to 15 mmHg or vice versa [40]. Rate of flow through the shell opening is governed by the equation:

$$Q = \frac{\pi r^4 \Delta P}{8 \eta l}, \tag{4}$$

where Q is the flow rate, r is the radius of the opening, ΔP is the pressure difference across the valve, l is the thickness of the valve and η is the viscosity of the fluid. Thus, the size of the opening can be modulated to determine the flow rate of the CSF though the valve. Given the approximate 13 ml/min average flow rate of the current shells valve over the $15 \rightarrow 7$ mmHg STB to rebound range, the valve would open on the order of 65 times per day for a total open time of ~15 min (Table 5). At this approximate rate, the 42,000 cycles tested in this paper simulates an average of 1.8 years *in vivo* of consistent STB shell valve opening and closing pressures.

5.4. Monitoring the shell: external and implantable monitoring

One of the main interests in using STB shells in the cerebral shunting application includes the possibility to monitor the mechanical displacement of valve actuation. We suggest two major non-invasive methods for such monitoring: clinical ultrasound and implantable constant monitoring mechanisms. Only ultrasound was examined in the methods and results of this paper, and implantable mechanisms remain theoretical, however, they do add to the importance of the current discussion.

5.4.1. Ultrasound

Preliminary work shows the ability for the large mechanical deformation afforded by the STB shell to be monitored using readily available clinical techniques such as ultrasound. The ability to actively monitor the shell for its position would be a powerful tool for clinical medicine. This may allow the physician to verify if there is flow or no flow in the shunt during various clinical maneuvers that artificially raise ICP, such as coughing or the Valsalva maneuver [41]. If STB events can be identified in a clinical setting, this would suggest that pressure is being transmitted though the shunt system and would rule out complete shunt blockages which account for 56.1% of shunt malfunctions [13]. Future work will further explore using ultrasound in the context of tissue and implantable form-factor shell casing.

5.4.2. Implantable mechanisms

These mechanisms would be implanted within the shunt valve casing to monitor the flow of CSF through the shunt and must include a sensing system, transmitter and a method of interrogation [42]. Three mechanisms we propose as viable options include: a luminous or electrical resistance measured across the valve, or making the shell from a piezoelectric polymer. There would be relatively large luminary and electrical resistance in the closed state and low resistance in the open state. Likewise, voltage would be generated by piezoelectric materials upon each valve actuation. These signals could be used to determine the number of valve openings, the current state of the valve, and establish a drainage baseline for each patient allowing for more personalized medicine. Future work will focus on refining a specific sensing mechanism to be implanted with the shell valve, and to develop an algorithm which would alert the patient or caregiver of flow abnormalities even before symptoms arise.

5.5. Infections

Infections occur as biofilms in shunt systems [43] and common prophylaxis methods include antimicrobial prophylaxis or antibiotic impregnated materials. Antibiotic impregnated catheters have

been shown as significant prognostic factors for shunt survival [44–48]. Unfortunately, no shunt valve on the market is fully antibiotic impregnated, leaving a vulnerable element in the shunt systems for bacterial colonization. STB shell valves can be made entirely from medical grade antibiotic impregnated Silastic® (Dow Corning, Midland, MI) material silicone or polyurethane type materials. Replacing non-impregnated valve with an impregnated valve system, resulting in the entire length of the shunt system being antibiotic impregnated, has the potential to significantly reduce shunt infection rates beyond the reduction enabled by impregnated catheters alone.

5.6. Observations & future work

It was noticed early on in testing that spoke lengths of 2 to 3 times longer than the thickness of the material was more likely to exhibit leaks of fluid at the slits rather than undergo STB phenomenon. More research should be focused at optimizing the characteristics of spoke parameters including spoke number and spoke length to reduce leakage and to optimize flow rates though open valves.

It was also noticed that as the valve rebounds, there is a possibility for backflow for fluid in the path of the moving shell membrane. This small back flow may prevent buildup of choroid plexus, blood and other sources of blockages from the proximal tip of the catheter located in the ventricles by applying a clearing backflow pressure wave on each rebound event. Further studies will be conducted with visible dye to ensure that particles from the distal end of the catheter do not traverse backwards up the shunt when a shell valve is used. *In vivo* animal models may also provide sufficient verification of the effects of the back-flow phenomenon. Backflow may be mitigated with the addition of an in-series, one-way check valve.

6. Conclusion

This study demonstrates that STB shells can be altered to act as valves that act in the physiologic range of ICP, while retaining a small form factor similar to cerebral shunts currently on the market. There is a range of shell parameters that can achieve these requirements, and these do not require extremes of manufacturing or material capabilities. Advantages of a STB shell valve compared to conventional valves include the ability to monitor the action of the valve for assessment of flow versus no flow in the clinical setting using standard ultrasound imaging techniques, and the possibility for antibiotic impregnation of the valve itself. Given the unique properties of the STB shell valve including large mechanical deformation, it may be feasible with future work to constantly monitor for flow anomalies using implantable sensors, transforming medical attention for shunt malfunction from reactionary to anticipatory. STB shells may also be helpful as a research tool to help elucidate *in vivo* charictaristics of CSF dynamics in hydrocephalus. Other potential medical applications for STB valves include cardiovascular valves, ureteric valves, and urethral valves.

Competing interests

None declared.

Conflict of interest

The authors have filed a patent relating to STB shell valve technology.

Ethical approval

None required.

Funding

Funding for this research was provided through a career development grant by the Department of Surgery at Dartmouth-Hitchcock Medical Center and the Cook Engineering Design Center at Dartmouth College.

Acknowledgements

The authors would like to thank Professor Ryan Halter for his support of innovation related to the present work.

Supplementary material

Supplementary material associated with this article can be found, in the online version, at doi:10.1016/j.medengphy.2018.12.024.

References

[1] Walker CT, Stone JJ, Jacobson M, Phillips V, Silberstein HJ. Indications for pediatric external ventricular drain placement and risk factors for conversion to a ventriculoperitoneal shunt. Pediatr Neurosurg 2012;48(6):342–7.
[2] Steiner LA, Andrews PJ. Monitoring the injured brain: ICP and CBF. Br J Anaesth 2006;97(1):26–38.
[3] Lee SC, Lueck CJ. Cerebrospinal fluid pressure in adults. J Neuroophthalmol 2014;34(3):278–83.
[4] Freeman WD. Management of intracranial pressure. Continuum (Minneap Minn) 2015;21(5 Neurocritical Care):1299–323.
[5] Jorgensen J, Williams C, Sarang-Sieminski A. Hydrocephalus and ventriculoperitoneal shunts: modes of failure and opportunities for improvement. Crit Rev Biomed Eng 2016;44(1–2):91–7.
[6] Maller VV, Agarwal A, Kanekar S. Imaging of ventricular shunts. Semin Ultrasound CT MRI 2016;37(2):159–73.
[7] El-Shafei IL, El-Shafei HI. The retrograde ventriculovenous shunts: the El-Shafei retrograde ventriculojugular and ventriculosinus shunts. Pediatr Neurosurg 2010;46(3):160–71.
[8] Demetriades AK, Haq I, Jarosz J, Mccormick D, Bassi S. The ventriculocholecystic shunt: two case reports and a review of the literature. Br J Neurosurg 2013;27(4):505–8.
[9] West CG. Ventriculovesical shunt. Technical note. J Neurosurg 1980;53(6):858–60.
[10] Simon TD, Riva-Cambrin J, Srivastava R, Bratton SL, Dean JM, Kestle JR. Hydrocephalus Clinical Research Network. Hospital care for children with hydrocephalus in the United States: utilization, charges, comorbidities, and deaths. J Neurosurg Pediatr 2008;1(2):131–7. doi:10.3171/PED/2008/1/2/131.
[11] Drake JM, Kestle JR, Milner R, Cinalli G, Boop F, Piatt J Jr, Haines S, Schiff SJ, Cochrane DD, Steinbok P, MacNeil N. Randomized trial of cerebrospinal fluid shunt valve design in pediatric hydrocephalus. Neurosurgery 1998;43(2):294–303 discussion 303–5.
[12] Stein SC, Guo W. Have we made progress in preventing shunt failure? A critical analysis. J Neurosurg Pediatr 2008;1(1):40–7.
[13] Sainte-Rose C, Piatt JH, Renier D, Pierre-Kahn A, Hirsch JF, Hoffman HJ, Humphreys RP, Hendrick EB. Mechanical complications in shunts. Pediatr Neurosurg 1991-1992;17(1):2–9.
[14] Kulkarni AV, Drake JM, Lamberti-Pasculli M. Cerebrospinal fluid shunt infection: a prospective study of risk factors. J Neurosurg 2001;94(2):195–201.
[15] Simon TD, Hall M, Riva-Cambrin J, Albert JE, Jeffries HE, Lafleur B, Dean JM, Kestle JR. Hydrocephalus Clinical Research Network. Infection rates following initial cerebrospinal fluid shunt placement across pediatric hospitals in the United States. J Neurosurg Pediatr 2009;4(2):156–65.
[16] Hanak BW, Bonow RH, Harris CA, Browd SR. Cerebrospinal fluid shunting complications in children. Pediatr Neurosurg 2017;52(6):381–400. doi:10.1159/000452840.
[17] Riva-Cambrin J, Kestle JR, Holubkov R, Butler J, Kulkarni AV, Drake J, Whitehead WE, Wellons JC 3rd, Shannon CN, Tamber MS, Limbrick DD Jr, Rozzelle C, Browd SR, Simon TD. Hydrocephalus Clinical Research Network. Risk factors for shunt malfunction in pediatric hydrocephalus: a multicenter prospective cohort study. J Neurosurg Pediatr 2016;17(4):382–90. doi:10.3171/2015.6.PEDS14670.
[18] Schievink WI. Spontaneous spinal cerebrospinal fluid leaks and intracranial hypotension. JAMA 2006;295(19):2286–96.
[19] Schievink WI. Misdiagnosis of spontaneous intracranial hypotension. Arch Neurol 2003;60(12):1713–18.
[20] van Dommelen P, Deurloo JA, Gooskens RH, Verkerk PH. Diagnostic accuracy of referral criteria for head circumference to detect hydrocephalus in the first year of life. Pediatr Neurol 2015;52(4):414–18. doi:10.1016/j.pediatrneurol.2014.06.024.
[21] Kim TY, Stewart G, Voth M, Moynihan JA, Brown L. Signs and symptoms of cerebrospinal fluid shunt malfunction in the pediatric emergency department. Pediatr Emerg Care 2006;22(1):28–34.

[22] Barnes NP, Jones SJ, Hayward RD, Harkness WJ, Thompson D. Ventriculoperitoneal shunt block: what are the best predictive clinical indicators? Arch Dis Child 2002;87(3):198–201.
[23] Kirkpatrick M, Engleman H, Minns RA. Symptoms and signs of progressive hydrocephalus. Arch Dis Child 1989;64(1):124–8.
[24] Vinchon M, Rekate H, Kulkarni AV. Pediatric hydrocephalus outcomes: a review. Fluids Barriers CNS 2012;9(1):18.
[25] "Shunt Malfunction Signs."; Shunt Malfunction Signs. Cincinnati Children's, J.W.J.
[26] Pople IK. Hydrocephalus and shunts: what the neurologist should know. J Neurol Neurosurg Psychiatry 2002;73(suppl 1):i17–22.
[27] Laurence KM, Coates S. The natural history of hydrocephalus. Detailed analysis of 182 unoperated cases. Arch Dis Child 1962;37:345–62.
[28] Piatt JH Jr, Garton HJ. Clinical diagnosis of ventriculoperitoneal shunt failure among children with hydrocephalus. Pediatr Emerg Care 2008;24(4):201–10.
[29] Spirig JM, Frank MN, Regli L, Stieglitz LH. Shunt age-related complications in adult patients with suspected shunt dysfunction. A recommended diagnostic workup. Acta Neurochir 2017;159(8):1421–8. doi:10.1007/s00701-017-3237-6.
[30] Drake JM, Kestle JR, Tuli S. CSF shunts 50 years on–past, present and future. Childs Nerv Syst 2000;16(10–11):800–4.
[31] Sellin JN, Cherian J, Barry JM, Ryan SL, Luerssen TG, Jea A. Utility of computed tomography or magnetic resonance imaging evaluation of ventricular morphology in suspected cerebrospinal fluid shunt malfunction. J Neurosurg Pediatr 2014;14(2):160–6. doi:10.3171/2014.4.PEDS13451.
[32] Bartynski WS, Valliappan S, Uselman JH, Spearman MP. The Adult Radiographic Shuntogram. Am J Neuroradiol 2000;21(4):721–6.
[33] da Costa Teixeira PB, et al. Mechanical behavior and stability of the internal membrane of the InCor ventricular assist device. Artif Organs 2001;25(11):912–21.
[34] Gonçalves PB, Pamplona D, Teixeira PBC, Jerusalmi, RLC, Cestari IA, Leirner AA. Dynamic non-linear behavior and stability of a ventricular assist device. Int J Solids Struct 2003;40(19):5017–35.
[35] Smooth-On, I. Silicone Rubber - Platinum Cure. June 25, 2017.
[36] Gent AN. On the relation between indentation hardness and Young's modulus. Rubber Chem Technol 1958;31(4):896–906.
[37] Iranthi M, Meththananda SP, Patel MP, Braden Michael. The relationship between Shore hardness of elastomeric dental materials and Young's modulus. Dent Mater 2009;25:956–9.
[38] Mokri B. The Monro–Kellie hypothesis: applications in CSF volume depletion. Neurology 2001;56(12):1746–8.
[39] Yasuda T, Tomita T, McLone DG, Donovan M. Measurement of cerebrospinal fluid output through external ventricular drainage in one hundred infants and children: correlation with cerebrospinal fluid production. Pediatr Neurosurg 2002;36(1):22–8.
[40] Kasprowicz M, Czosnyka M, Czosnyka Z, Momjian S, Smielewski P, Junlewicz H, Pickard JD. Hysteresis of the cerebrospinal pressure-volume curve in hydrocephalus. In: Kuroiwa T, et al., editors. Brain Edema XII: Proceedings of the twelfth international symposium, Hakone, Japan. Springer; 2003. p. 529–32.
[41] Prabhakar H, Bithal PK, Suri A, Rath GP, Dash HH. Intracranial pressure changes during Valsalva manoeuvre in patients undergoing a neuroendoscopic procedure. Minim Invasive Neurosurg 2007;50(2):98–101.
[42] Khaled SR, Sameoto D, Evoy S. A review of piezoelectric polymers as functional materials for electromechanical transducers. Smart Mater Struct 2014;23(3):033001.
[43] Jimenez-Mejias ME, Garcia-Cabrera E. [Infection of cerebrospinal fluid shunt systems]. Enferm Infecc Microbiol Clin 2008;26(4):240–51.
[44] Iglesias S, Ros B, Martín Á, Carrasco A, Segura M, Ros A, Rius F, Arráez MÁ. Factors related to shunt survival in paediatric hydrocephalus. Could failure be avoided? Neurocirugia (Astur) 2017;28(4):159–66. doi:10.1016/j.neucir.2016.12.004.
[45] Klimo P Jr, Thompson CJ, Ragel BT, Boop FA. Antibiotic-impregnated shunt systems versus standard shunt systems: a meta- and cost-savings analysis. J Neurosurg Pediatr 2011;8(6):600–12. doi:10.3171/2011.8.PEDS11346.
[46] Yang B, et al. Prevention of infection by antibiotic-impregnated shunts after pediatric hydrocephalus treatment: a single center, retrospective study in China. Clin Neurol Neurosurg 2016;151:92–5.
[47] Klimo P Jr, Thompson CJ, Baird LC, Flannery AM. Pediatric Hydrocephalus Systematic Review and Evidence-Based Guidelines Task Force. Pediatric hydrocephalus: systematic literature review and evidence-based guidelines. Part 7: antibiotic-impregnated shunt systems versus conventional shunts in children: a systematic review and meta-analysis. J Neurosurg Pediatr 2014;14(Suppl 1):53–9. doi:10.3171/2014.7.PEDS14327.
[48] Bayston R, Grove N, Siegel J, Lawellin D, Barsham S. Prevention of hydrocephalus shunt catheter colonisation in vitro by impregnation with antimicrobials. J Neurol Neurosurg Psychiatry 1989;52(5):605–9.